Computational Analysis of the 2415-3S Airfoil Aerodynamic Performance

Luis Velazquez-Araque[1] and Jiří Nožička[2]

[1]Department of Mechanical Engineering
National University of Táchira, San Cristóbal 5001, Venezuela
[2] Department of Mechanical Engineering
Czech Technical University in Prague, Prague 16607, Czech Republic

ABSTRACT

This paper deals with the numerical simulation of the two-dimensional, incompressible, steady air flow past an airfoil for a solar powered unmanned aerial vehicle (UAV) with internal propulsion system. This airfoil results from a NACA 2415 four digits family base airfoil modification [7] and has a propulsive outlet with the shape of a step on the suction surface. The analysis involved the airfoil's aerodynamic performance which meant obtaining lift, drag and pitching moment coefficient curves as a function of the angle of attack (AOA) for the condition where the engine of the UAV is turned off called the gliding condition and also for the blowing propulsive condition by means computational fluid dynamics. The computational domain has been discretised using a structured mesh of 188 x 200 tetrahedral elements. The RNG k-ε model is utilized to describe the turbulent flow process as it was followed in [5]. The simulations were held at a Reynolds number of 300000. Results allowed obtaining lift and drag forces and pitching moment coefficient and also the location of the separation and reattachment points in some cases by means of the wall shear stress on the suction surface as well as velocity contours and streamlines for both conditions at different angles of attack, from 0 to 16 degrees with the smallest increment of 4 degrees. Finally, results from both cases were compared and the influence of the propulsive flow on the aerodynamic characteristics of the airfoil has been analysed turning out that it improves significantly the performance of the airfoil reaching values up to 1,8 times in terms of lift at high angles of attack.

Keywords - lift; drag; pitching moment; unmanned aerial vehicle; CFD.

1. AIRFOIL TESTED

The 2415-3S airfoil (Figure 1), has been previously designed for the solar UAV focusing on several parameters of common commercial UAV's manufactures such as total wingspan, weight, flight velocity and others. It comes from a NACA four digits family airfoil, the NACA 2415 (Figure 2) [4]. It has an abrupt step on the suction side, located at 30% of the chord from the leading edge. This step simulates the blowing propulsive outlet of the wing in normal flight conditions. Since solar panels must be placed on the wings, it is possible to see the large and almost flat area for placing them past the blowing outlet.
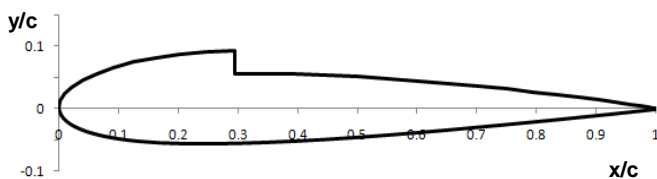
Figure 1. 2415-3S airfoil.
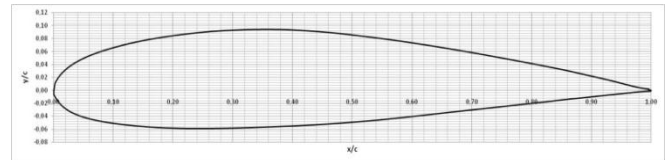
Figure 2. NACA 2415 airfoil.

2. COMPUTATIONAL DOMAIN

Something very important in this part is the choice of the domain, because it is formed by real borders such as the upper and lower surfaces of the airfoil and also by imaginary borders which enclose the external environment. The domain extends from 8 chord lengths upstream to 20 chord lengths downstream according to [1], an also 8 chord lengths for the upper and lower heights. The fluid flow simulated is air with a Reynolds number of 3.10^5. In Figure 3 it is possible to see the geometry of the domain for the 2415-3S airfoil.
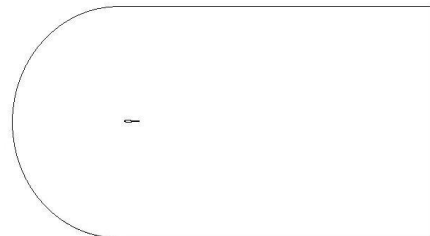
Figure 3. Computational domain for numerical simulations.

3. DISCRETIZATION OF THE DOMAIN

The geometry shown in Figure 3 is discretised using a structured mesh of 188 x 200 tetrahedral elements, this mesh has been also supplemented with very small elements in the vicinity of the surface of the airfoil forming a boundary layer with a grow factor of 1.2. References when creating the mesh were followed in [3], therefore the created mesh had a size change of 2.66 and an equisize skew of 0.348.
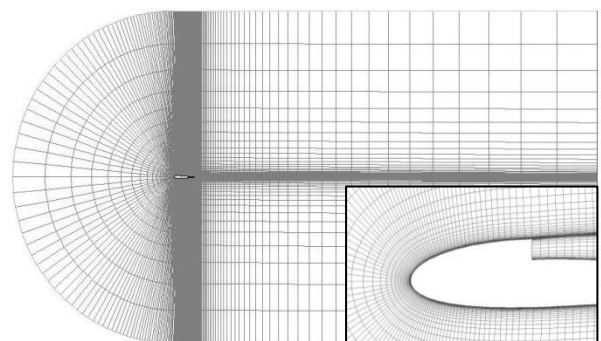
Figure 4. A mesh used for the numerical simulation.

The domain and the mesh were created using the commercial software GAMBIT, version 2.3. In order to obtain the lift and drag as a function angle of attack, single meshes were created for 0, 4, 8, 12 and 16 degrees and for every airfoil, thus there were created a total of 20 meshes (Figure 4).

Then, from the governing equations, the discretization of the domain and using the finite volume method based on finite elements, a discrete set of algebraic equations is set which solution is obtained as coupled, iteratively, using the commercial solver ANSYS FLUENT, version 12.0 using a scheme of second order upwind.

4. TURBULENCE MODEL

The k-ε model is derived from the Navier-Stokes equations and it is one of the simplest complete models of turbulence with two-equation models in which the solution of two separate transport equations allows the turbulent velocity and length scales to be independently determined. The standard k-ε model in ANSYS FLUENT falls within this class of models and has become very used for practical engineering flow calculations. It is a semi-empirical model. It is robust, economic, and presents reasonable accuracy for a wide range of turbulent flows. The chosen turbulence model was the RNG k-ε. The RNG (renormalization group theory) is an improvement of this model of turbulence because it provides an analytically derived differential formula for effective viscosity that accounts for low-Reynolds-number effects. Therefore it is more accurate and reliable for a wider class of flows.

5. BOUNDARY CONDITIONS

At the inlet it is specified the air absolute velocity magnitude and also its components; in this case the velocity is parallel to the horizontal axis, therefore it does not have any component in the ordinates. Concerning turbulence, it was also specified the turbulence intensity of 1,3 % in accordance to [2] and also the turbulent length scale. The upper and lower surfaces of the airfoil are set as walls. At the outlet it is specified the pressure as the atmospheric pressure. For the lateral walls of the domain they are set as symmetry.

6. GOVERNING EQUATIONS

Since this problem does not involve heat transfer nor compressibility the equation for energy conservation is not required, therefore the most important equations such as conservation of mass, momentum and the RNG k-ε turbulence model equations are used.

7. RESULTS AND ANALYSIS

Gliding Condition

In Figures 5 – 8, it is possible to see numerical lift coefficient (C_L) versus AOA, drag coefficient (C_D) versus AOA, C_L versus C_D and pitching moment coefficient (C_m) versus AOA for the 2415-3S airfoil for the condition where there is not flow through the blowing outlet. Curves from the original NACA 2415 airfoil have been included from [5] for further comparisons.
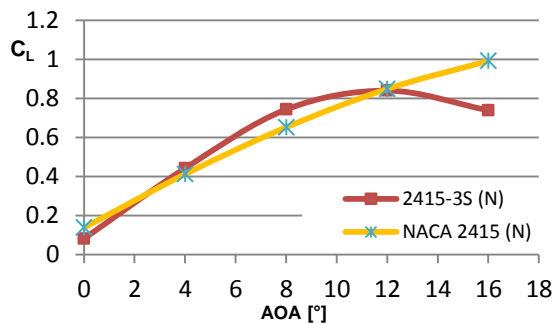
Figure. 5. Numerical lift coefficient for 2415-3S and NACA 2415 airfoils.

Concerning lift coefficient shown in Figure. 5, it can be observed the lift slope presented by the 2415-3S airfoil which was simulated at a Reynolds number of 310528 for a flow velocity of 20m/s, the stall region starts at 8 degrees of AOA with a stall point of $C_L = 0,84$ at 12 degrees of AOA, it is clear that the stall region starts at a lower AOA since the NACA 2415 presents the beginning of the stall region at 15 degrees. This airfoil at these conditions also presents higher values of C_L compared to the NACA 2415 between 4 and 12 degrees of AOA.
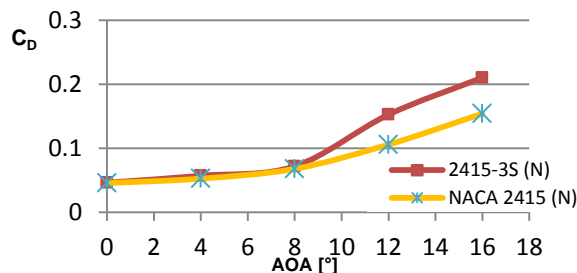
Figure 6. Numerical drag coefficient for 2415-3S and NACA 2415 airfoils.

In Figure 6 above, it is possible to see that the drag coefficient observed in the 2415-3S airfoil approaches to values similar to the NACA 2415 for AOA between 0 and 8 degrees. From this point, the values of drag coefficient increase rapidly. This behavior may indicate that the flow reattaches the airfoil surface after the step until 8 degrees of AOA, however this will be confirmed with the wall shear stress charts and streamlines which will be analyzed later. At 0 degrees of AOA both airfoils present a similar value of C_D around 0,05.
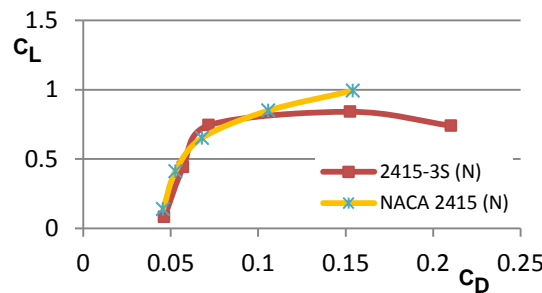
Figure 7. Numerical polar graph for 2415-3S and NACA 2415 airfoils.

The polar diagram shown in Figure 7 indicates that the airfoil 2415-3S has a good aerodynamic performance since it is very similar to NACA's 2415 from 0 to 10 degrees of AOA, however this performance decreases at high angles of attack, specifically from 10 degrees.

Concerning pitching moment coefficient at the leading edge, results shown in Figure 8 indicate that values of the 2415-3S airfoil present discrepancies but the behavior in general is similar to NACA's 2415 airfoil until 12 degrees of angle of attack.
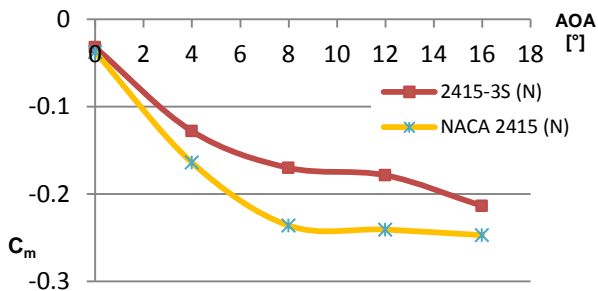
Figure 8. Numerical pitching moment coefficient for 2415-3S and NACA 2415 airfoils.

In Figure 9, it is possible to see the numerical wall shear stress on the suction surface along the chord line for the 2415-3S airfoil for the gliding condition; these images allow observing points of separation and reattachment of the flow. A shear stress is applied parallel or tangential to a face of a material. Any real fluids (liquids and gases included) moving along a solid surface will incur a shear stress on that surface. That is the reason why the wall shear stress is considered an indicative of separation of flow because when it is equal to zero, it means that the flow is not attached to the surface of the airfoil [6]. After this point, values of shear stress are different of zero and the separation region begins. In the case of reattachment of flow, it is noticed when the values of wall shear stress reach zero again, and the area between these two points is the separation region, in this region, the values of wall shear stress are negative, this can be seen if only the x-component of the wall shear stress is plotted but for a better observation, it was decided to plot the resultant wall shear stress, where all values are always positive.

It can be seen that the flow detaches at the location of the step at all AOA excepting at 16 degrees where the flow detaches before the step at 23 percent of the chord. At 0 and 4 degrees of AOA the flow reattaches after the step at locations of 56 and 62,5 percent of the chord, respetively. At 12 and 16 degrees of AOA the flow does not reattach to the surface of the 2415-3S airfoil.
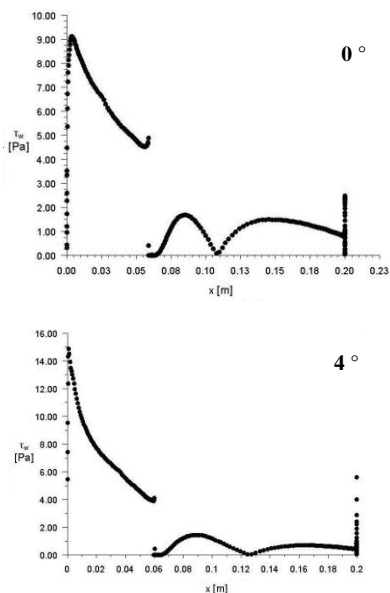
Figure 9. Wall shear stress of the 2415-3S airfoil at gliding condition for different AOA.
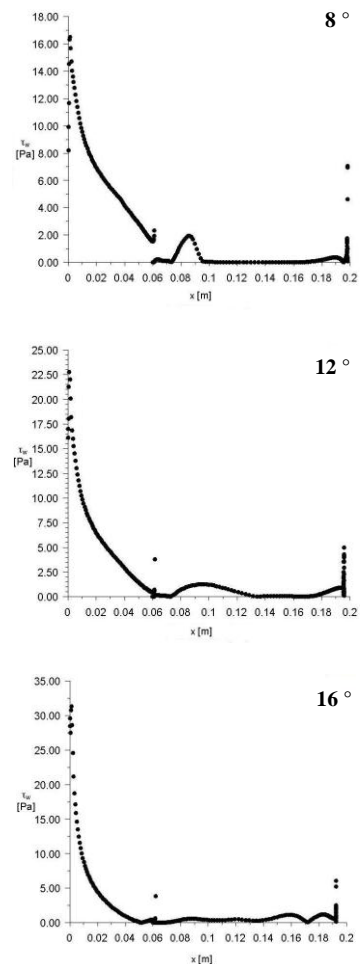
Figure 9. Wall shear stress of the 2415-3S airfoil at gliding condition for different AOA.

In Figure 10 it is possible to observe the flow field as velocity contours of the air flow past the 2415-3S airfoil. This is the first numerical graphical approach to the behavior of the air flow past the airfoil tested. Here it is observable the velocity changes in the selected domain; in our case the most important is to observe this phenomenon near the surface of the model. However these pictures do not show clearly the separation and reattachment points.
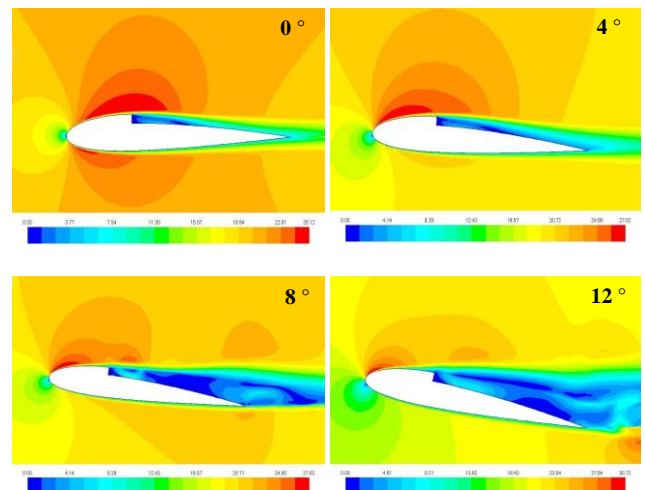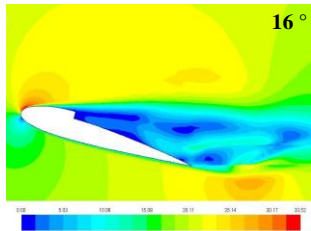
Figure 10. Velocity contours of the 2415-3S airfoil at gliding condition for different AOA.

Observing the flow fields for all AOA in Figure 10, it is possible to notice that for 8 degrees of AOA within the separation region, zones of high velocity which may indicate the presence of vortices due to the turbulence provoked by the high velocity of the flow and the sudden change in the geometry of the airfoil. This phenomenon will be observed in more detail below when analyzing the streamlines.

In Figure 11, it is possible to see the streamlines of the flow past the 2415-3S airfoil.
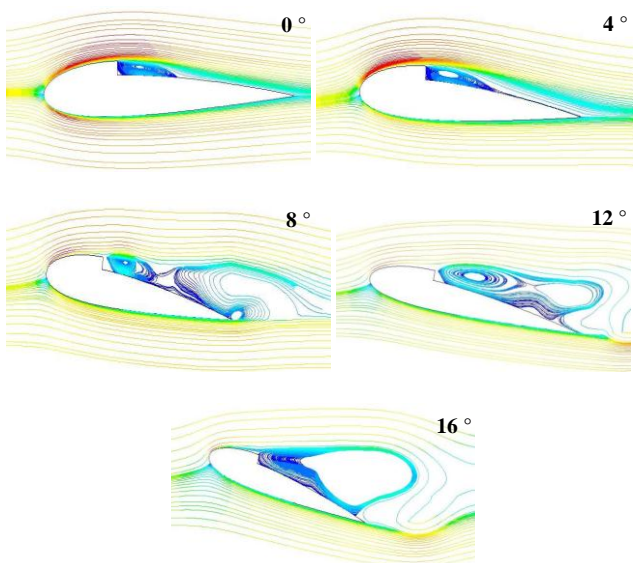
Figure 11. Streamlines of the 2415-3S airfoil at gliding condition for different AOA.

In Figure 11, it is observed that the flow is fully attached to the suction surface of the airfoil until the step where separation of flow occurs. This phenomenon occurs for almost all AOA. The spatial extension of the separation region can be detected by exploring the wall shear stress along the surface of the airfoil (Figure 9). Inside this region, it is possible to observe that the adverse pressure gradient causes a reversed flow and this becomes into a counter-rotating vortex. Then the flow reattaches again and remains in contact with the surface until the trailing edge, this reattachment was observed from 0 to 4 degrees of AOA. At 8 and 12 degrees of angle of attack, the flow does not reattach to the surface but in this case two vortices appear within the separation region due to the turbulences provoked by the high velocity of the flow. At 16 degrees of AOA, the separation region is huge but in this case it begins at certain distance before the step.

Propulsive Condition

In order to develop the new numerical simulation involving the blowing scenario, only one boundary condition was changed and it was the step which was not set as "wall" anymore but as

"velocity inlet" and the value of this parameter was introduced as normal to the boundary, the introduced value was 30 m/s.

In Figures 12 - 15, it is possible to see numerical C_L versus AOA, C_D versus AOA, C_L versus C_D and C_m versus AOA for the 2415-3S airfoil for the condition where air at a velocity of 30 m/s flows through the blowing outlet. Previous curves of the 2415-3S for the gliding condition and curves of the original NACA 2415 airfoil have been included for further comparisons.
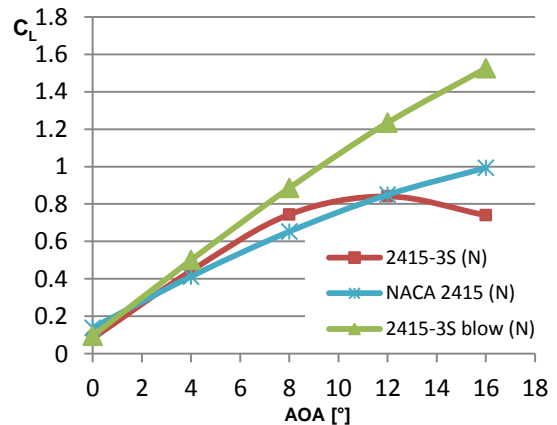
Figure 12. Numerical lift coefficient for 2415-3S airfoil for blowing and gliding conditions and NACA 2415 airfoil.

In Figure 12, the values of the lift coefficient for the 2415-3S at this new condition are similar to the ones for the gliding condition at very low angles of attack up to 4 degrees but from this point, the C_L increases rapidly and progressively with a higher slope and reaching values up to 1,5 times bigger than the original NACA 2415. The lift curve does not present a stall region in the range of studied angles of attack, what makes think that the flow is very attached to the surface of the airfoil for AOA even higher than 16 degrees. However this will be discussed when analyzing the wall shear stress graphs and streamlines.
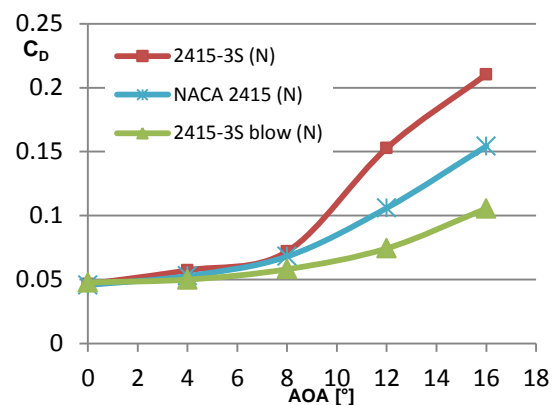
Figure 13. Numerical drag coefficient for 2415-3S airfoil for blowing and gliding conditions and NACA 2415 airfoil.

Concerning drag coefficient, shown in Figure 13, it is possible to see that values of C_D are low and similar for all cases at low angles of attack until 7 degrees, after this point the drag of the 2415-3S at the gliding condition increases rapidly and the drag of the original NACA 2415 does so but moderately. The C_D of the 2415-3S at the blowing condition increases as well but very moderately less that all other cases reaching a maximum of 0,1055 at the highest AOA, this indicates that the air blowing through the outlet does not exert a big influence on the drag

because the flow seems to be attached at every moment to the surface of the airfoil.
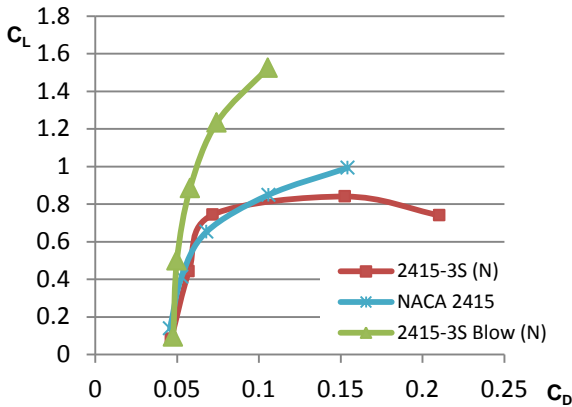
Figure 14. Numerical polar graph for 2415-3S airfoil for blowing and gliding conditions and NACA 2415 airfoil.

The polar graph shown in Figure 14 summarizes all the aspects previously observed in Figures 12 and 13. It is clear that the effect of blowing maximizes the aerodynamic performance of the airfoil and it can be seen in the polar curve for the 2415-3S which is completely concave, also for low angles of attack it is almost vertical, which indicates that the drag does not vary very much and the lift increases rapidly. Being the original NACA's 2415 aerodynamic performance the main goal during the modification of the airfoil, it has been greatly improved by the blowing effect.
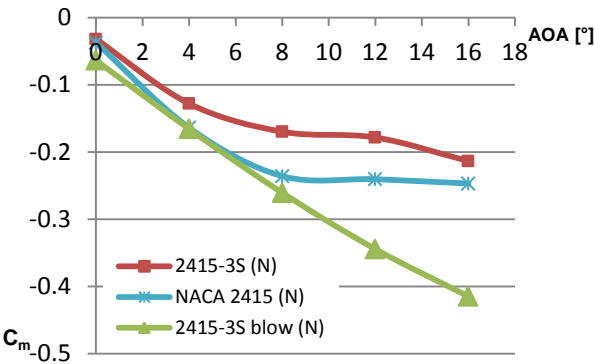
Figure 15. Numerical pitching moment coefficient for 2415-3S airfoil for blowing and gliding conditions and NACA 2415 airfoil.

Concerning pitching moment coefficient at the leading edge, results shown in Figure 15 indicate that the C_m for the 2415-3S at the blowing condition increases almost directly proportional to the angle of attack. Comparing to the NACA 2415 airfoil the behaviour is similar until 8 degrees of AOA where it stabilizes and the other still increases reaching a maximum of 0,415 in magnitude at 16 degrees of angle of attack.

In Figure 16, it is possible to see the numerical wall shear stress on the suction surface along the chord line for the 2415-3S airfoil under the blowing condition; these images allow observing points of separation and reattachment of the flow. It can be observed, according to the wall shear stress behaviour that the flow never detaches from the surface of the airfoil at any tested angle of attack, there is not present any separation region and high values of AOA could be reached without stalling. However it is important to note some aspects; the initial value of the wall shear stress at the leading edge, which is high and then decreases towards the location of the blowing outlet where a sudden rise is

present in this point because of the flow through the outlet, reaching much higher values and then it decreases towards the trailing edge. Besides, the initial value of the wall shear stress at the leading edge increases with the angle of attack while the behavior after the step remains constant no matter the AOA.
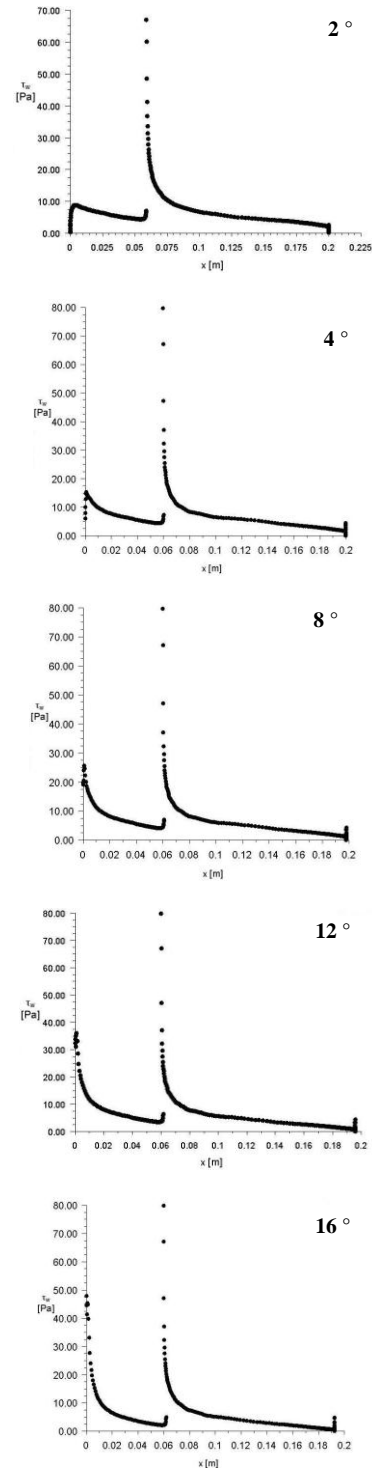
Figure 16. Wall shear stress of the 2415-3S airfoil at blowing condition for different AOA.

In Figure 17, it is possible to observe the flow field as velocity contours of the air flow past the 2415-3S airfoil under the blowing condition.
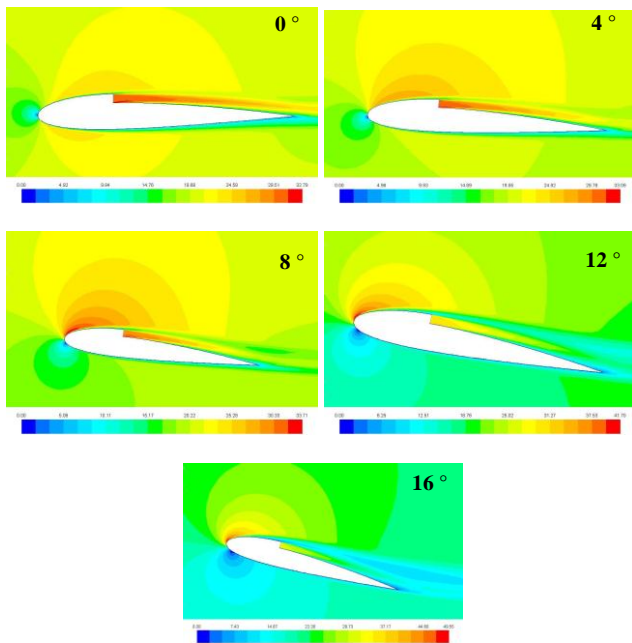
Figure 17. Velocity contours of the 2415-3S airfoil at blowing condition for different AOA.

Comparing the flow fields obtained for the blowing scenario in Figure 17 to the ones obtained for the gliding condition, it is possible to see the zone of highest velocity just next to the boundary called "blowing", and this is the locus of the propulsion. No presence of regions with a velocity of 0 m/s besides the stagnation point at the leading edge, therefore no regions of separation were observed at any angle of attack.

In Figure 18, it is possible to see the streamlines of the flow past the 2415-3S airfoil under the blowing condition.
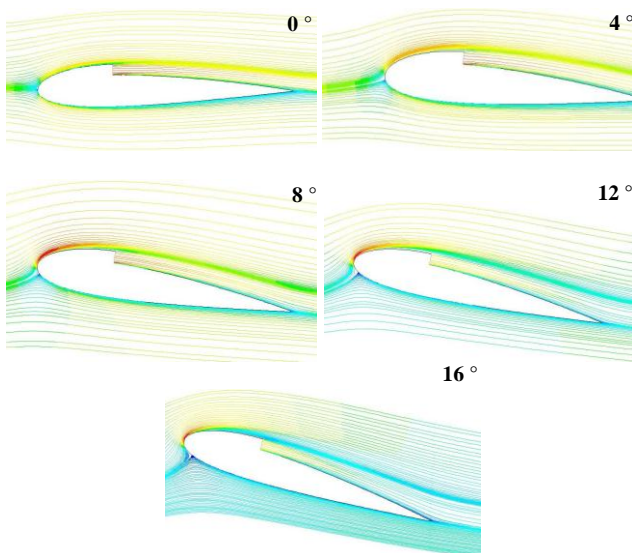
Figure 18. Streamlines of the 2415-3S airfoil at blowing condition for different AOA.

Concerning streamlines, it is possible to observe in Figure 18 the flow along the airfoil for the blowing scenario, where these ones look very well distributed, now next to the blowing outlet, streamlines are fully attached to the upper surface until the trailing edge, filling all the spots which are formed when there is not flow through the outlet. No vortices are present. Streamlines look parallel to the surface at every angle of attack, which helps to believe that much higher AOA's can be reached without approaching to the stall condition.

8. CONCLUSION

By means of the use of CFD it has been possible to obtain lift, drag and pitching moment coefficients and also the flow field of air past a new designed airfoil, the 2415-3S. It was also possible to obtain the location of separation and reattachment points in some cases for different angles of attack. Two conditions (gliding and propulsive) were analyzed through an exhaustive comparison, turning out that the aerodynamic performance of the airfoil increases at the blowing propulsive condition reaching values up to 1,8 times in terms of lift at high angles of attack.

9. REFERENCES

[1] Malan P., Suluksna K., Juntasaro E., Calibrating the γ-Re_θ Transition Model for Commercial CFD, in *The 47th AIAA Aerospace Sciences Meeting, 2009.*

[2] Nožička J., http://profily.fs.cvut.cz/, Laboratory of Department of Fluid Dynamics and Power Engineering of the CTU in Prague. Section Airfoils and Straight Blade Cascades.

[3] Rhie C.M., Chow W.L., Numerical Study of the Turbulent Flow Past an Airfoil with Trailing Edge Separation, *AIAA Journal*, Vol. 21, No. 11, 1983.

[4] Selig M.S., Lyon C.A., Giguere P., Ninham C., Guglielmo J.J., *Summary of Low-Speed Airfoil Data*, Vol. 2, Viginia Beach, SoarTech Publications, 1996.

[5] Rhie C.M., Chow W.L., Numerical Study of the Turbulent Flow Past an Airfoil with Trailing Edge Separation, *AIAA Journal*, Vol. 21, No. 11, 1983.

[6] Velazquez L., Nožička J., Numerical Simulation of the Fluid Flow past an Airfoil for an Unmanned Aerial Vehicle, in *The 22nd International Symposium on Transport Phenomena*. Delft, the Netherlands, 2011.

[7] Velazquez L., Nožička J, Kulhanek R., Oil and Smoke Flow Visualization past Two-Dimensional Airfoils for an Unmanned Aerial Vehicle, in *The 11th Asian Symposium of Visualization*. Niigata, Japan. 2011.

[8] Velazquez L., Nožička J., Vavřín J., Experimental Measurement of the Aerodynamic Characteristics of Two-Dimensional Airfoils for an Unmanned Aerial Vehicle, in *Experimental Fluid Mechanics 2010*. Liberec, 2010.